

# Magnetogel Nanospheres Composed of Cisplatin-Loaded Alginate/ $\beta$ -Cyclodextrin as Controlled Release Drug Delivery

Ali Darini<sup>1</sup>, Touba Eslaminejad<sup>2</sup> , Seyed Noroddin Nematollahi Mahani<sup>3</sup> , Mehdi Ansari<sup>4\*</sup> 

<sup>1</sup>Department of Nanotechnology, Pharmaceutical Sciences Branch, Islamic Azad University (IAUPS), Tehran, Iran.

<sup>2</sup>Pharmaceutics Research Center, Institute of Neuropharmacology, Kerman University of Medical Sciences, Kerman, Iran.

<sup>3</sup>Department of Anatomy, Afzalipour School of Medicine, Kerman University of Medical Sciences, Kerman, Iran.

<sup>4</sup>Neuroscience Research Center, Institute of Neuropharmacology, Kerman University of Medical Sciences, Kerman, Iran.

## Article info

### Article History:

Received: 30 July 2018

Revised: 11 June 2019

Accepted: 15 June 2019

published: 24 Oct. 2019

### Keywords:

- Alginate
- Beta-cyclodextrin
- Cancer
- Cisplatin
- Controlled release
- Drug delivery systems
- Magnetic nanoparticles

## Abstract

**Purpose:** The main aim of the present study was to design, fabrication and physicochemical characteristics of the magnetogel nanospheres as carriers for Cisplatin in the *in vitro* environment.

**Methods:** Magnetic nanospheres were synthesized by using a chemical co-precipitation method and coated by sodium alginate through double emulsion method. Then cisplatin was encapsulated into  $\beta$ -cyclodextrin -sodium alginate grafted magnetic nanospheres. The physicochemical properties of the sodium alginate grafted magnetic nanospheres were characterized by using FT-IR, particle size analyzing, vibrating sample magnetometry, thermogravimetric and SEM analysis. Also the drug entrapment efficiency, content and *in vitro* release profile were investigated.

**Results:** Size distribution results revealed that the particles size was distributed in the range of  $50 \pm$  nm. Also morphological properties showed that particles are separated and spherical with the grafted layers of the polymer. The release profile data were in the acceptable range compared to the blank (cisplatin solution).

**Conclusion:** It could be concluded that the sodium alginate grafted magnetic nanospheres could act as a slow and controlled release system to deliver cisplatin.

## Introduction

Cancer incidence and mortality rates increase year by year, making it a serious threat to human health. Conventional therapy methods cannot completely eliminate the cancer cell. In this part, chemotherapy is efficient adjuvant approaches to removing residual cancer cells and preventing tumor recurrence and metastasis, but their application is limited because of their serious side effects. Thereof, controlled drug delivery systems that allow releasing of drugs just at the desired site (cancerous cells) for extended periods time are needed. Furthermore, the significant effects of the targeted drug delivery lie to minimize toxic effects. Currently, cis-diammine dichloroplatinum (CP), as the first platinum-containing a chemotherapeutic agent is widely used in the treatment of solid tumors. Cell division is arrested by CP to prevent tumor growth and induces programmed cell death. Unfortunately, CP displayed serious side effects such as nephrotoxicity, ototoxicity, neurotoxicity, nausea, and vomiting because of systemic administration, which limits its clinical utilization.<sup>1,2</sup> Thereof, to avoid these side effects CP is loaded on the nanocarriers to enhance

permeability retention effects. Nanotechnology plays a unique role in cancer diagnosis and therapy<sup>3</sup> and provide controlled drug release with increased tumor selectivity and decreased toxicity.<sup>4,5</sup> Applying magnetic nanoparticles in the presence of an external magnetic field focus on the target tissue has already been demonstrated as a promising approach for the specific delivery of therapeutic agents.<sup>6,7</sup> Iron oxide nanoparticles are widely used as contrast agents and drug carriers in preclinical and clinical settings.<sup>8</sup>

Polymeric delivery systems have the potential to maintain therapeutic levels of a drug, to reduce side effects and to facilitate the delivery of drugs with short *in vivo* half-lives.<sup>9</sup> Because of several unique properties of alginate, it was allowed to use for the entrapment the delivery of a variety of biological agents.<sup>10</sup> Alginate is non-toxic, biodegradable, low in cost, readily available, and mucoadhesive, biocompatible, and non-immunogenic substance.<sup>11,12</sup> It is an anionic polymer and composed of two types of uronic acid monomers distributed as blocks of 1 $\rightarrow$ 4 linked  $\alpha$ -L-guluronic acid (G) or  $\beta$ -D-mannuronic acid (M), as well as heteropolymeric mixed sequences (G-M, usually alternating). Cyclodextrins (CDs), a family of

\*Corresponding Author: Mehdi Ansari, Tel: +98 3431325022, Fax: +98 3431325003, Email: mansari@kmu.ac.ir

macrocyclic oligosaccharides linked by  $\alpha$ -1, 4 glycosidic bonds, have been widely studied in various fields. Among them,  $\alpha$ -,  $\beta$ -, and  $\gamma$ -CDs are the most common members, which are composed of 6, 7, and 8 glucose units, consecutively.<sup>13,14</sup> The hydrophobic cavity of CDs gives them inclusion capacity with a diversity of compounds from small molecules, ions, proteins, and oligonucleotides. To further improve the pharmaceutical features of native CDs, chemically modified CDs have been synthesized.<sup>15-17</sup> Therefore, in the present work CP was conjugated with  $\beta$ -CD and then loaded on the  $\text{Fe}_3\text{O}_4$ /alginate nanospheres. Physicochemical characteristics of the new synthesis particles were determined by using FT-IR, TGA, SEM, and TEM. Finally, drug entrapment efficiency (%), drug content (% w/w) and the *in vitro* release profile of CP-magnetic nanospheres were determined.

## Materials and Methods

### Materials

CP hydrochloride was purchased from Sobhan Oncology Co., Tehran, Iran.  $\beta$ -CD was purchased from Walker Chemie, Munich, Germany, *o*-Phenylenediamine and potassium dihydrogen orthophosphate, dimethylformamide (DMF), ammonium hydroxide (25%) and sodium hydroxide flakes were purchased from Merck, Darmstadt, Germany.  $\text{FeCl}_2 \cdot 4\text{H}_2\text{O}$ ,  $\text{FeCl}_3 \cdot 6\text{H}_2\text{O}$ , and sodium alginate were purchased from Sigma-Aldrich, Louis, MO, USA, and used without further purification except when mentioned specifically. Dulbecco's modified eagle's medium F12 (DMEM), fetal bovine serum (FBS), penicillin-streptomycin (100  $\mu\text{g}/\text{mL}$ ), phosphate-buffered saline (PBS), MTT (3-(4, 5-dimethylthiazol-2-yl)-2, 5-diphenyltetrazolium bromide), and dimethyl sulphoxide (DMSO) were purchased from the Sigma Aldrich Company, Mo, USA.

### Methods

#### Preparation of $\text{Fe}_3\text{O}_4$ nanoparticle

$\text{Fe}_3\text{O}_4$  nanoparticles were prepared by using co-precipitated method with some modification.<sup>18</sup> Briefly, 35 mL of 1 mol/L  $\text{FeCl}_2$  and 1.5 mol/L  $\text{FeCl}_3$  suspensions were added into a three-necked flask to make the molar ratio of  $\text{Fe}^{2+}$  and  $\text{Fe}^{3+}$  maintaining 1:1.5, and was stirred under nitrogen atmospheres. Then ammonia (25% w/w) was added to regulate the pH value to 11 at 60°C and the dark suspension was incubated on vigorous stirring at 80°C for 1 h. Finally, the  $\text{Fe}_3\text{O}_4$  black precipitate was allowed to cool to room temperature (25°C) and the separated by centrifugation at 6000 rpm for 20 min. The dark precipitate was lyophilized and stored in desiccators for later experiments.<sup>19</sup>

#### Preparation of CP encapsulated superparamagnetic alginate/ $\beta$ -cyclodextrin nanospheres ( $\text{Fe}_3\text{O}_4$ /A/ $\beta$ -CD/CP)

Firstly a stock solution of 20 mg of cisplatin was prepared in DMF and then diluted with 4.2 mL of deionized water

(DDW), sonicated for 12 min to have a uniform suspension and kept on the dark conditions (wrap in the Aluminum foil).  $\beta$ -CD (76 mg) was dissolved in 20 mL of DDW. Then CP suspension was added drop-wise to the  $\beta$ -CD solution and sonicated at 22°C for 10 min to encapsulate CP in the  $\beta$ -CD. CP encapsulated  $\beta$ -CD colloids were drop-wise to the sodium alginate colloid (160 mg in the DDW) under stirring (A/ $\beta$ -CD/CP).  $\text{Fe}_3\text{O}_4$  (48 mg) was suspended in a ratio of 2:1 (V/V) of ethanol: DDW in an ultrasonic bath at 22°C for 10 min. Finally, A/ $\beta$ -CD/CP composite was drop-wise into  $\text{Fe}_3\text{O}_4$  suspension under agitation. The suspension was vibrated in an ultrasonic bath and stirred vigorously by a homogenizer simultaneously at room temperature for 30 min. Then, 14 mL of 0.01 M  $\text{CaCl}_2$  solution as cross-linker and 3.2 mL of 0.12 M  $\text{NaHCO}_3$  solution were poured into the mixture and stirred for 2 h. The suspension was separated by a permanent magnet and washed with ethanol and distilled water and then freeze-dried for later experiments.<sup>19</sup>

#### Characterization of the fabricated particles

FT-IR spectra from  $\beta$ -CD, CP, sodium alginate,  $\text{Fe}_3\text{O}_4$ ,  $\text{Fe}_3\text{O}_4$ /A/ $\beta$ -CD and  $\text{Fe}_3\text{O}_4$ /A/ $\beta$ -CD/CP were recorded by a Fourier transforms infrared spectrophotometer (Tensor 27, Bruker Co.). Particle size, poly dispersity index, and zeta potential were measured using dynamic light scattering with a Nano-S90 Zeta Sizer (Malvern Instruments, Worcestershire, UK). All experiments were carried out at 25°C and repeated three times. The morphological studies of  $\text{Fe}_3\text{O}_4$ /A/ $\beta$ -CD and  $\text{Fe}_3\text{O}_4$ /A/ $\beta$ -CD/CP were observed by transmission electron microscopy (TEM, CM-10 PHILIPS, 80 kV) and scanning electron microscopy (FE-SEM, MIRA 3 XMU, Tescan USA Inc.). The magnetization curves of  $\text{Fe}_3\text{O}_4$ ,  $\text{Fe}_3\text{O}_4$ /A/ $\beta$ -CD, and  $\text{Fe}_3\text{O}_4$ /A/ $\beta$ -CD/CP were measured with a vibrating sample magnetometer (VSM-7300, Meghnatis Kavir Co., Kashan Iran). The differential thermal analysis (DTA) coupled with thermogravimetric (TG) analysis of  $\text{Fe}_3\text{O}_4$ /A/ $\beta$ -CD and  $\text{Fe}_3\text{O}_4$ /A/ $\beta$ -CD/CP were observed by a TG-DTA apparatus (NETZSCH-GERÄTEBAU GMBH-STA 409 PC LXXX, Kerman, Iran) by heating the samples from 25 to 900°C at a heating rate of 10°C per min under an  $\text{N}_2$  atmosphere.

#### Drug loading measurements

One milliliter of  $\text{Fe}_3\text{O}_4$ /A/ $\beta$ -CD/CP suspension was reached to 10 mL by DDW and then the free drug was separated by centrifugation at 6000 rpm for 15 min. Then after the free drug was measured according ortho-phenylenediamine method.<sup>1</sup> Briefly, one ml of the supernatant was transferred to a 10 mL tube with a screw cap, and the measurement of the absorbance of the CP was done at 705 nm. Finally, the amount of the drug that was loaded on the particles was calculated by using the following formula:

Drug loaded (%) = total amount of drug / amount of the

drug that was recovered from the supernatant.

### *In vitro* release profile of CP

Dynamic dialysis method was used to investigate the *in vitro* release of CP. Briefly,  $\text{Fe}_3\text{O}_4/\text{A}/\beta\text{-CD}/\text{CP}$  and CP suspension in phosphate buffered saline (0.1 M) were poured into two dialysis bags (Millipore, molecular weight cutoff 12 kDa, USA) separately, and suspended into 100 mL phosphate buffered saline (0.1 M) with pH 7.4 at 37°C under constant stirring. The receptor compartment was sealed to avoid evaporation of the receptor phase. At predetermined time intervals, 1 mL of the released CP-PBS suspension outside of the dialysis bags were withdrawn and replaced with equal volume of the fresh receptor phase to complete the initial volume. Then CP absorbance was quantified by UV-Vis measurement and the released amount of CP was calculated according to the CP standard curve analysis.

### Cell viability assay

MCF-7 cells ( $10^4$ ) were maintained in DMEM supplemented with 10% FBS and 1% penicillin/streptomycin on each well of 96-well culture dish and incubated at 37°C in a humidified atmosphere with 5%  $\text{CO}_2$  for 24 h. 100  $\mu\text{L}$  of the  $\text{Fe}_3\text{O}_4/\text{A}/\beta\text{-CD}/\text{CP}$  composites at the various concentrations of 0.005, 0.043, 0.425, 4.25 and 42.5  $\mu\text{g}/\text{mL}$  were applied to each well, followed by 24 h incubation. The next day 10  $\mu\text{L}$  of MTT solution was added to each well and kept in the incubator conditions for 3 h. The absorbance of the samples was measured by ELISA reader (BioTek® Elx 800) at 490 nm wavelength and the reference of 630 nm. Absorbance of non-treated cells (as control) was estimated as 100% viability and the treated cells were calculated according to that. The survival rate (%) was calculated according to the following equation<sup>20</sup>:

$$\% \text{ Survival rate} = (\text{OD in treatment group} / \text{OD in control group}) \times 100.$$

### Statistical analysis

Data were presented as mean  $\pm$  SD while experiments were performed in triplicate. SPSS software version 15 for Windows (SPSS Inc., Chicago) was utilized for statistical analysis. The differences between the groups in the *in vitro* release profile of CP were determined by employing *t* test analysis. Microsoft Office Excel 2010 was also used as appropriate statistical software.

## Results and Discussion

### Characterization of fabricated particles

#### FT-IR studies

The FT-IR spectra of CP,  $\beta\text{-CD}$ , sodium alginate,  $\text{Fe}_3\text{O}_4$ ,  $\text{Fe}_3\text{O}_4/\text{A}/\beta\text{-CD}$  and  $\text{Fe}_3\text{O}_4/\text{A}/\beta\text{-CD}/\text{CP}$  are presented in Figure 1. Absorption peak presented at 1645.85  $\text{cm}^{-1}$ , belonged to the stretching vibration of the carbonyl group, this absorption also presents in the  $\beta\text{-CD}$ , which confirmed the presence of  $\beta\text{-CD}$  in the final product.

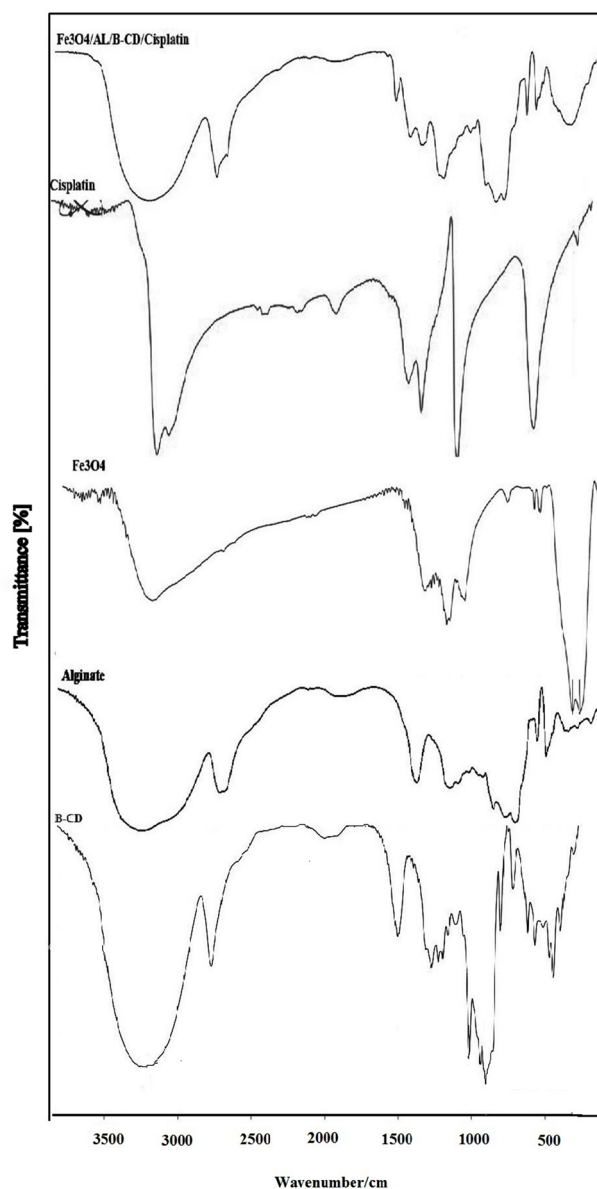


**Figure 1.** FT-IR spectra of cisplatin;  $\beta\text{-CD}$ ; Sodium Alginate (SA);  $\text{Fe}_3\text{O}_4$  and  $\text{Fe}_3\text{O}_4/\text{SA}/\beta\text{-CD}/\text{CP}$ .

The absorption band at 2924.42  $\text{cm}^{-1}$ , can be attributed to  $-\text{CH}$  stretching vibration in sodium alginate and  $\beta\text{-CD}$ . The band at 3283.56  $\text{cm}^{-1}$ , can be assigned to  $-\text{NH}_2$  stretching, and according to the peak at 3419.11  $\text{cm}^{-1}$  in  $\text{Fe}_3\text{O}_4/\beta\text{-CD}/\text{CP}$  that related to N-H stretching, and can be inferred that the absorption peak corroborated the attendance of CP is in the final composition. These results indicated to conformity mentioned compounds in pure form with  $\text{Fe}_3\text{O}_4/\beta\text{-CD}/\text{CP}$  and confirmed the presence of these compounds in the final composite structure.

#### Particle size and zeta potential

Size distribution and zeta potential of  $\text{Fe}_3\text{O}_4/\beta\text{-CD}$  and  $\text{Fe}_3\text{O}_4/\beta\text{-CD}/\text{CP}$  are shown in Figure 2. The average diameter of  $\text{Fe}_3\text{O}_4/\beta\text{-CD}$  was 57 nm while the mean size of  $\text{Fe}_3\text{O}_4/\beta\text{-CD}/\text{CP}$  was 65 nm. Z-potential of the

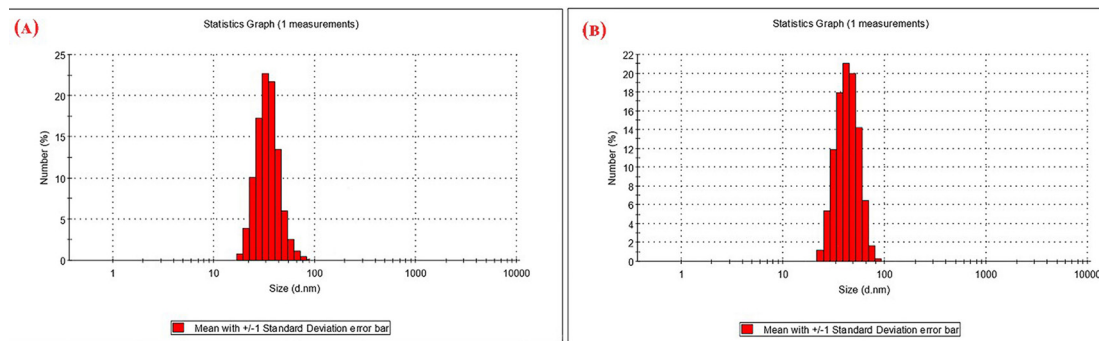


Figure 2. Particle size distribution of (A);  $\text{Fe}_3\text{O}_4/\text{SA}/\beta\text{-CD}$  and (B);  $\text{Fe}_3\text{O}_4/\text{SA}/\beta\text{-CD}/\text{CP}$ .

$\text{Fe}_3\text{O}_4/\text{A}/\beta\text{-CD}$  was -16, while  $\zeta$ -potential of the  $\text{Fe}_3\text{O}_4/\text{A}/\beta\text{-CD}/\text{CP}$  was decreased to -10 by two peaks with sizes of -4 and -30 respectively, which could be represented an appropriate repulsion between particles and particle size stability.

#### FE-SEM studies

Results from FE-SEM analysis performed to examine the morphological aspect and size of  $\text{Fe}_3\text{O}_4/\text{A}/\beta\text{-CD}$  and  $\text{Fe}_3\text{O}_4/\text{A}/\beta\text{-CD}/\text{CP}$  and are depicted in Figure 3. According to the FE-SEM images, the mean particle size was about 50 nm and the shape of nanoparticles was elliptical to roughly spherical. Results from surface analysis of nanoparticles indicated a lack of accumulation of nanoparticles that is one of the criteria for the proper functioning of the nanoparticles.<sup>21,22</sup> EDX analyses performed on the surface of  $\text{Fe}_3\text{O}_4/\text{A}/\beta\text{-CD}$  and  $\text{Fe}_3\text{O}_4/\text{A}/\beta\text{-CD}/\text{CP}$  clearly indicated the presence of Ca, Fe, O, C, Cl and Na (Figure 3 C and D). The peaks of Fe indicated the excitation of electrons in this atom in atomic layers M and L and move them to the lower layers.

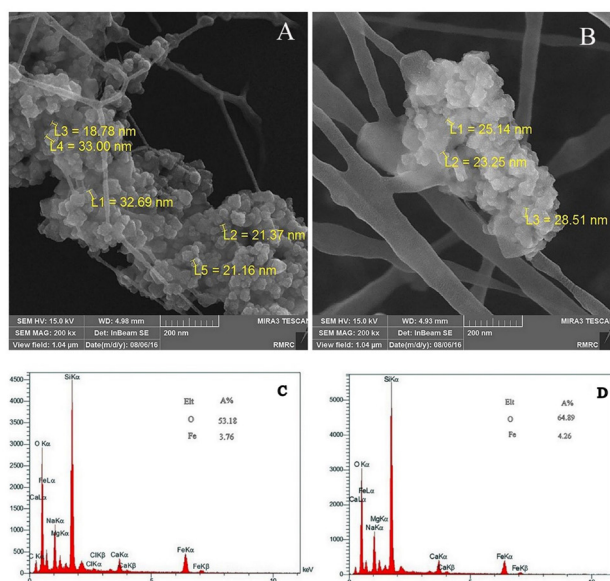


Figure 3. SEM micrographs of (A);  $\text{Fe}_3\text{O}_4/\text{SA}/\beta\text{-CD}$  and (B);  $\text{Fe}_3\text{O}_4/\text{SA}/\beta\text{-CD}/\text{CP}$  and EDX analysis results of (C);  $\text{Fe}_3\text{O}_4/\text{SA}/\beta\text{-CD}$  and (D);  $\text{Fe}_3\text{O}_4/\text{SA}/\beta\text{-CD}/\text{CP}$  respectively.

#### TEM studies

The TEM images of  $\text{Fe}_3\text{O}_4/\text{A}/\beta\text{-CD}$ , and  $\text{Fe}_3\text{O}_4/\text{A}/\beta\text{-CD}/\text{CP}$  nanoparticles are given in Figure 4. The average diameter of  $\text{Fe}_3\text{O}_4$  nanoparticles was about 36 nm with a spherical shape. According to images, it could be seen that  $\text{Fe}_3\text{O}_4/\text{A}/\beta\text{-CD}$  and  $\text{Fe}_3\text{O}_4/\text{A}/\beta\text{-CD}/\text{CP}$  have the spherical morphology and the mean diameter of nanoparticles was approximately 50 nm. As for being observed, the black crystalline core with a diameter about 36 nm is surrounded by gray layer with a diameter about 7 nm. It can assume that the preparation of magnetic supports was successful.

#### VSM studies

Magnetization curves (M-H loop) of  $\text{Fe}_3\text{O}_4$ ,  $\text{Fe}_3\text{O}_4/\text{A}/\beta\text{-CD}$ , and  $\text{Fe}_3\text{O}_4/\text{A}/\beta\text{-CD}/\text{CP}$  are illustrated in Figure 5. The saturation magnetization values of 72, 40, and 42 emu/g were measured for  $\text{Fe}_3\text{O}_4$ ,  $\text{Fe}_3\text{O}_4/\text{A}/\beta\text{-CD}$ , and  $\text{Fe}_3\text{O}_4/\text{A}/\beta\text{-CD}/\text{CP}$ , respectively. As a result, these magnetic supports were used for carrying CP could be separated from the reaction medium rapidly and easily in an external magnetic field.<sup>23</sup> Moreover, there was no hysteresis in the magnetization with both remanence and coercivity being zero, proving that these magnetic nanoparticles were superparamagnetic.<sup>24</sup> Therefore, these magnetic supports could respond to an applied magnetic field without any permanent magnetization and redispersed rapidly when the magnetic field disappeared. The prepared supports showed well super paramagnetic and better saturation magnetization.

#### STA studies

The TG-DTA analyses of  $\text{Fe}_3\text{O}_4/\text{A}/\beta\text{-CD}$  and  $\text{Fe}_3\text{O}_4/\text{SA}/\beta\text{-CD}/\text{CP}$  respectively.

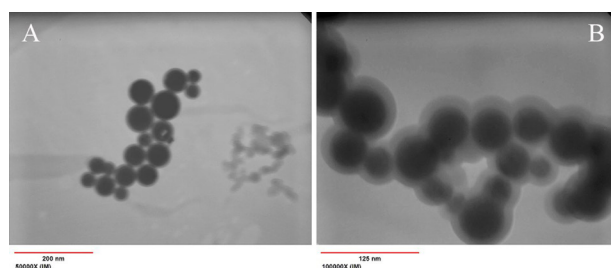


Figure 4. TEM micrographs of synthesized nanoparticles of (A);  $\text{Fe}_3\text{O}_4/\text{SA}/\beta\text{-CD}$  and (B);  $\text{Fe}_3\text{O}_4/\text{SA}/\beta\text{-CD}/\text{CP}$  respectively.

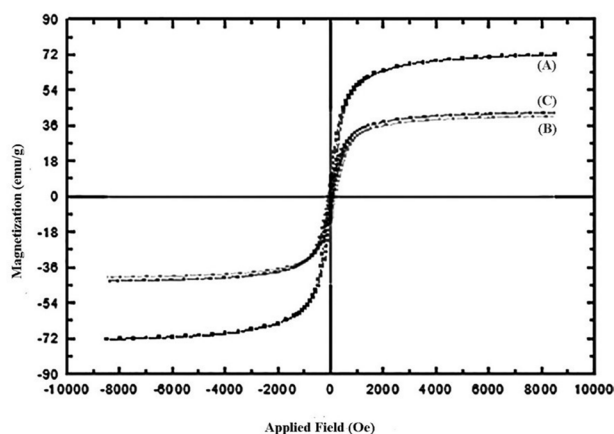


Figure 5. Magnetization hysteresis loop of (A);  $\text{Fe}_3\text{O}_4$ ; (B);  $\text{Fe}_3\text{O}_4/\text{SA}/\beta\text{-CD}$  and (C);  $\text{Fe}_3\text{O}_4/\text{SA}/\beta\text{-CD}/\text{CP}$  respectively.

$\beta\text{-CD}/\text{CP}$  nanospheres are given in Figure 6. The TG curve was observed five stages of weight loss in a temperature range of (30-100°C), (100-200°C), (200-300°C), (300-400°C) and (400-470°C) respectively. The first stage of weight loss occurred in the range temperature of 30-100°C due to water evaporation surface of the nanospheres,<sup>25</sup> and weight loss in the later stages was due to evaporation of useful water and organic compounds in the super paramagnetic nanospheres.<sup>26,27</sup> That its weight loss was consistent with the presence of two exothermic peaks

around 300°C and 430°C (Figure 6 A) for  $\text{Fe}_3\text{O}_4/\text{A}/\beta\text{-CD}$  and 300°C and 420°C (Figure 6 B) for  $\text{Fe}_3\text{O}_4/\text{A}/\beta\text{-CD}/\text{CP}$  in the DTA curve, respectively.<sup>28</sup>

#### Drug loading measurements

Loading percentage of CP was the remaining amount on the system compared to the initial amount (50  $\mu\text{g}$ ). Data showed that about 85% of the drug was loaded on the  $\text{Fe}_3\text{O}_4/\text{A}/\beta\text{-CD}$  nanospheres. Thus it represents an excellent loading capabilities drug delivery system, which in turn is remarkable.<sup>29,30</sup>

#### Drug release measurement

The release profiles of CP (blank) and  $\text{Fe}_3\text{O}_4/\text{A}/\beta\text{-CD}/\text{CP}$  suspensions after 300 min are shown in Figure 7. Results are expressed as released percent (mean  $\pm$  SD) at different times. Clearly, blank exhibited very rapid releases in PBS solution; about 100% of drug over 1 h while  $\text{Fe}_3\text{O}_4/\text{A}/\beta\text{-CD}/\text{CP}$  composite showed a significant delay in the release, and only 30% of CP was released in PBS solution at the same period of time and very sustained release during 5 h. This is because of the drug deposited on the outer surface of the composites in the early hours and sustained release of the encapsulated drug in a long time. That confirms the appropriate capability and performance of the controlled drug delivery system that was designed.<sup>31</sup> Drug nanoparticles showed the ability of full release of

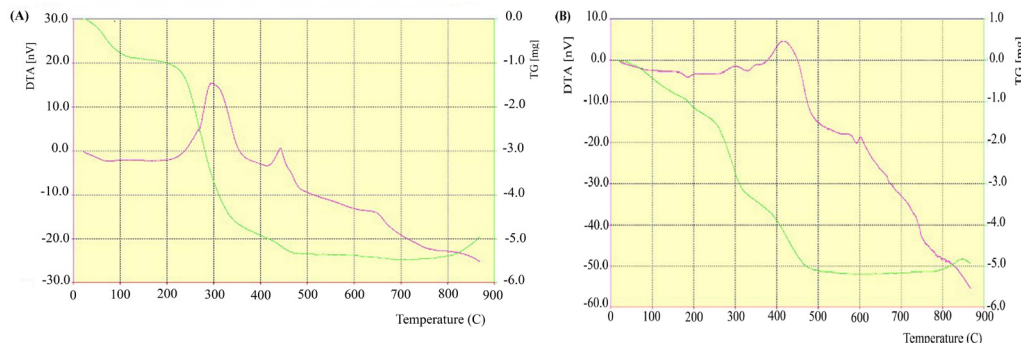


Figure 6. TG-DTA analysis of (A);  $\text{Fe}_3\text{O}_4/\text{SA}/\beta\text{-CD}$  and (B);  $\text{Fe}_3\text{O}_4/\text{SA}/\beta\text{-CD}/\text{CP}$  respectively.

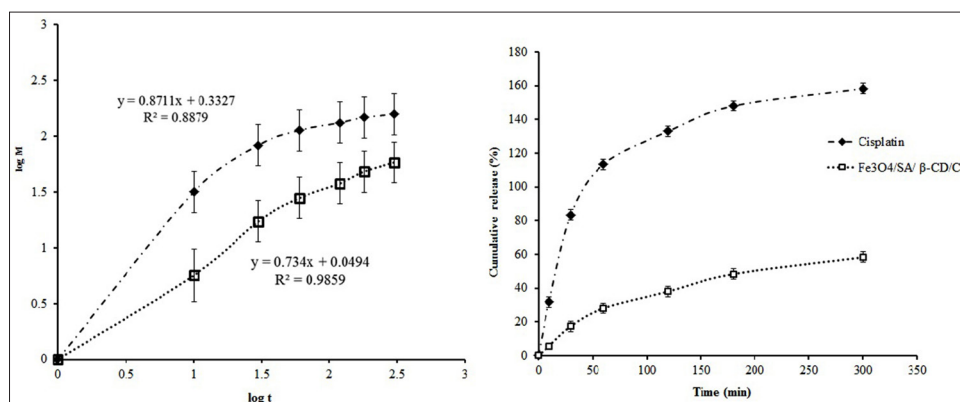


Figure 7. Cumulative release of CP from  $\text{Fe}_3\text{O}_4/\text{SA}/\beta\text{-CD}$  composite after 300 min.

drug due to small size and larger surface area. The quantity of cumulated release of drug during 5 h was near 60%. The quantification of the  $R^2$  was used to determine the type of kinetic release. Zero-order, first-order, Peppas–Korsmeyer, Higuchi, Weibull, and Hixon–Crowell are kinetic models that are used in *in vitro* release study.<sup>32</sup> According to the  $R^2=0.9845$  obtained from the *in vitro* release the Peppas–Korsmeyer model was the best fit with cisplatin release from  $\text{Fe}_3\text{O}_4/\text{A}/\beta\text{-CD}$  composites.

#### Cytotoxicity assay

The toxicity of various concentrations of encapsulated cisplatin in  $\text{Fe}_3\text{O}_4/\text{A}/\beta\text{-CD}$  composite was evaluated by using MTT tests to quantify cell viability (Figure 8). Results showed that as the concentration of encapsulated cisplatin rose from zero to 0.141  $\mu\text{M}$ , the survival rate was decreased dose- dependently with an  $\text{IC}_{50}$  value of 0.06  $\mu\text{M}$ , while the mean  $\text{IC}_{50}$  value of free cisplatin was obtained 5.75 and 8.6  $\mu\text{M}$ .<sup>33</sup> This means that  $\text{Fe}_3\text{O}_4/\text{A}/\beta\text{-CD}/\text{CP}$  composite could better decrease the cell progression during to the time of the incubation; this effect may be related to the drug release by delay.

#### Conclusion

In general, it can be concluded that cisplatin was loaded sufficiently and efficiently on the  $\text{Fe}_3\text{O}_4/\text{A}/\beta\text{-CD}$  composites which could be released in a sustained, slow and controlled mannered. These drug delivery systems have a potential to response to the external magnetic stimuli which may be applied in the targeted cancer chemotherapy.

#### Conflict of Interest

There is no conflict of interest.

#### Ethical Issues

Not applicable.

#### Acknowledgments

The work has been kindly supported by the Kerman University of Medical Sciences (KMU) of Iran.

#### References

- Zhang W, Tung CH. Cisplatin Cross-Linked Multifunctional Nanodrugplexes For Combination Therapy. *Acs Appl Mater Interfaces* 2017;9(10):8547-55. doi: : 10.1021/Acsami.6b16500
- Takimoto Y, Imai T, Kondo M, Hanada Y, Uno A, Ishida Y, et al. Cisplatin-induced toxicity decreases the mouse vestibulo-ocular reflex. *Toxicol Lett* 2016;262:49-54. doi: : 10.1016/J.Toxlet.2016.09.009
- Hammond PT. Shooting for the moon: nanoscale approaches to cancer. *Acs Nano* 2016;10(2):1711-3. doi: : 10.1021/Acsnano.6b01095
- Spring BQ, Sears RB, Zheng LZ, Mai Z, Watanabe R, Sherwood ME, et al. A photoactivable multi-inhibitor nanoliposome for tumour control and simultaneous inhibition of treatment escape pathways. *Nat Nanotechnol*

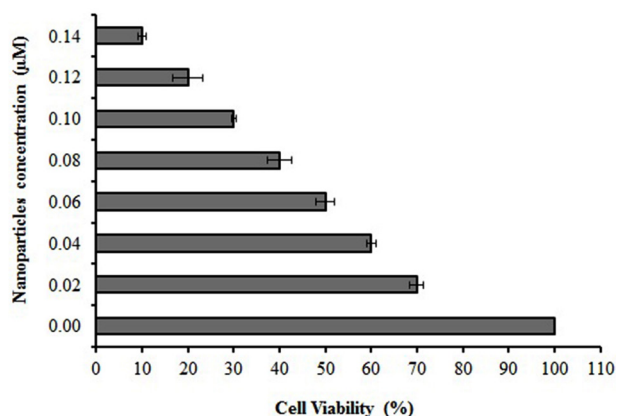


**Figure 8.** Dose-dependent inhibition properties of  $\text{Fe}_3\text{O}_4/\text{SA}/\beta\text{-CD}/\text{CP}$  nanospheres after 24 h incubation, Data presented as mean  $\pm$  standard deviation (n=3).

- 2016;11:378-87. doi: : 10.1038/Nnano.2015.311
- Nascimento AV, Singh A, Bousbaa H, Ferreira D, Sarmento B, Amiji MM. Overcoming cisplatin resistance in non-small cell lung cancer with Mad2 silencing siRNA delivered systemically using EGFR-targeted chitosan nanoparticles. *Acta Biomater* 2017;47:71-80. doi: : 10.1016/J.Actbio.2016.09.045
- Mikhaylov G, Mikac U, Magaeva AA, Itin VI, Naiden EP, Psakhye I, et al. Ferri-liposomes as an MRI-visible drug-delivery system for targeting tumours and their microenvironment. *Nat Nanotechnol* 2011;6(9):594-602. doi: : 10.1038/Nnano.2011.112.
- Arruebo M, Fernández-Pacheco R, Ibarra MR, Santamaría J. Magnetic nanoparticles for drug delivery. *Nano Today* 2007;2(3):22-32. doi: : 10.1016/S1748-0132(07)70084-1
- Zanganeh S, Hutter G, Spitler R, Lenkov O, Mahmoudi M, Shaw A, et al. Iron oxide nanoparticles inhibit tumour growth by inducing pro-inflammatory macrophage polarization in tumour tissues. *Nat Nanotechnol* 2016;11(11):986-94. doi: : 10.1038/Nnano.2016.168.
- Ulbrich K, Holá K, Šubr V, Bakandritsos A, Tuček J, Zbořil R. Targeted drug delivery with polymers and magnetic nanoparticles: covalent and noncovalent approaches, release control, and clinical studies. *Chem Rev* 2016;116(9):5338-431. doi: : 10.1021/Acs.Chemrev.5b00589.
- Ciofani G, Raffa V, Menciassi A, Cuschieri A, Micera S. Magnetic alginate microspheres: system for the position controlled delivery of nerve growth factor. *Biomaterials* 2009;30(2):517-27. doi: : 10.1007/S10544-008-9258-4
- Paques JB, Van Der Linden E, Van Rijn CJ, Sagis LM. Preparation methods of alginate nanoparticles. *Adv Colloid Interface Sci* 2014;209:163-71. doi: : 10.1016/J.Cis.2014.03.009
- Pawar SN, Edgar KJ. Alginate derivatization: a review of chemistry, properties and applications. *Biomaterials* 2012;33(11):3279-305. doi: : 10.1016/J.Biomaterials.2012.01.007
- Yu Y, Wang Q, Yuan J, Fan X, Wang P. A novel approach for grafting of  $\beta$ -cyclodextrin onto wool via laccase/ tempo oxidation. *Carbohydr Polym* 2016;153:463-70. doi: : 10.1016/J.Carbpol.2016.08.003
- Skiba M, Wouessidjewe D, Puisieux F, Duchêne D, Gulik

- A. Characterization of amphiphilic  $\beta$ -cyclodextrin nanospheres. *Int J Pharm* 1996;142(1):121-4. doi: : 10.1016/0378-5173(96)04653-4
15. Abdolmaleki A, Mallakpour S, Mahmoudian M, Sabzalian MR. A new polyamide adjusted triazinyl- $\beta$ -cyclodextrin side group embedded magnetic nanoparticles for bacterial capture. *Chem Eng J* 2017;309:321-9. doi: : 10.1016/J.Cej.2016.10.063
16. Davis ME, Brewster ME. Cyclodextrin-based pharmaceuticals: past, present and future. *Nat Rev Drug Discov* 2004;3(12):1023-35. doi: : 10.1038/Nrd1576
17. Rodrigues LB, Martins AO, Ribeiro-Filho J, Cesário FR, E Castro FF, de Albuquerque TR, et al. Anti-inflammatory activity of the essential oil obtained from *Ocimum basilicum* complexed with  $\beta$ -cyclodextrin ( $\beta$ -CD) in mice. *Food Chem Toxicol* 2017. doi: : 10.1016/J.Fct.2017.02.027
18. Ghandoor EH, Zidan HM, Khalil MM, Ismail MIM. Synthesis and some physical properties of magnetite (Fe<sub>3</sub>O<sub>4</sub>) nanoparticles. *Int J Electrochem Sci* 2012;7(6):5734-45. doi: : 10.13140/Rg.2.1.2745.9442
19. Liu X, Chen X, Li Y, Wang X, Peng X, Zhu W. Preparation of superparamagnetic Fe<sub>3</sub>O<sub>4</sub>@alginate/chitosan nanospheres for *Candida rugosa* lipase immobilization and utilization of layer-by-layer assembly to enhance the stability of immobilized lipase. *Acs Appl Mater Interfaces* 2012;4(10):5169-78. doi: : 10.1021/Am301104c
20. Eslaminejad T, Nematollahi-Mahani SN, Ansari M. Cationic  $\beta$ -cyclodextrin-chitosan conjugates as potential carrier for pmcherry-c1 gene delivery. *Mol Biotechnol* 2016;58(4):287-98. doi: : 10.1007/S12033-016-9927-0
21. Qasim M, Asghar K, Das D. Facile synthesis of Fe<sub>3</sub>O<sub>4</sub> and multifunctional Fe<sub>3</sub>O<sub>4</sub>@ albumen nanoparticles for biomedical applications. *Aip Conf Proc* 2017;1832(1):050116. doi: : 10.1063/1.4980349
22. Su CH, Velusamy P, Kumar GV, Adhikary S, Pandian K, Anbu P. Studies of antibacterial efficacy of different biopolymer protected silver nanoparticles synthesized under reflux condition. *Jmost* 2017;1128:718-23. doi: : 10.1016/J.Molstruc.2016.09.045
23. Raja P, Yadavalli T, Ravi D, Therese HA, Ramasamy C, Hayakawa Y. Synthesis and magnetic properties of gadolinium substituted zinc ferrites. *Mater Lett* 2017;188:406-8. doi: : 10.1016/J.Matlet.2016.11.083
24. Mikler C, Chaudhary V, Borkar T, Soni V, Choudhuri D, Ramanujan R, et al. Laser additive processing of Ni-Fe-V and Ni-Fe-Mo permalloys: microstructure and magnetic properties. *Mater Lett* 2017;192:9-11. doi: : 10.1016/J.Matlet.2017.01.059
25. Oliveira GF, Andrade RC, Trindade MA, Andrade HM, Carvalho CT. Thermogravimetric and spectroscopic study (TG-DTA/FT-IR) of activated carbon from the renewable biomass source babassu. *Quim Nova* 2017;40(3):284-92. doi: : 10.21577/0100-4042.20160191
26. Domán A, Madarász J, László K. In situ evolved gas analysis assisted thermogravimetric (TG-FTIR and TG/DTA-MS) studies on non-activated copper benzene-1,3,5-tricarboxylate. *Thermochim Acta* 2017;647:62-9. doi: : 10.1016/J.Tca.2016.11.013
27. Ohadi M, Dehghannoudeh G, Foroortanfar H, Shakibaie M, Rajaei M. Investigation of the structural, physicochemical properties, and aggregation behavior of lipopeptide biosurfactant produced by *Acinetobacter junii* B6. *Int J Biol Macromol* 2018;112:712-9. doi: : 10.1016/J.Ijbiomac.2018.01.209
28. Bai Y, Zhou X, Zhan C, Ma L, Yuan Y, Wu C, et al. 3D Hierarchical nano-flake/micro-flower iron fluoride with hydration water induced tunnels for secondary lithium battery cathodes. *Nano Energy* 2017;32:10-8. doi: : 10.1016/J.Nanoen.2016.12.017
29. Tan J, Cho TJ, Tsai D-H, Liu J, Pettibone JM, You R, et al. Surface modification of cisplatin-complexed gold nanoparticles and its influence on colloidal stability, drug loading, and drug release. *Langmuir* 2018;34(1):154-63. doi: : 10.1021/Acs.Langmuir.7b02354
30. Huang Y-Q, Zhang R, Zhao Y-K, Chen H, Jiang R-C, Liu X-F, et al. Self- Self-assembled nanoparticles based on a cationic conjugated polymer/hyaluronan-cisplatin complex as a multifunctional platform for simultaneous tumor-targeting cell imaging and drug delivery. *N J Chem* 2017;41:4998-5006. doi: : 10.1021/Acsnano.6b01095
31. Zhao H, Xu J, Wan J, Geng S, Li H, Peng X, et al. Cisplatin-cisplatin-directed coordination-crosslinking nanogels with thermo/pH-sensitive triblock polymers: improvement on chemotherapeutic efficacy via sustained release and drug retention. *Nanoscale* 2017;9(18):5859-71. doi: : 10.1039/C7nr01097d
32. Hamishehkar H, Bahadori MB, Vandghanooni S, Eskandani M, Nakhband A, Eskandani M. Preparation, characterization and anti-proliferative effects of sclareol-loaded solid lipid nanoparticles on A549 human lung epithelial cancer cells. *J Drug Deliv Sci Technol* 2018;45:272-80. doi: : 10.1016/J.Jddst.2018.02.017
33. Suberu JO, Romero-Canelón I, Sullivan N, Lapkin AA, Barker GC. Comparative cytotoxicity of artemisinin and cisplatin and their interactions with chlorogenic acids in MCF7 breast cancer cells. *ChemMedChem* 2014;9(12):2791-7. doi: : 10.1002/Cmdc.201402285